Journal of Electroanalytical Chemistry 775 (2016) 64–71

Contents lists available at ScienceDirect

Journal of Electroanalytical Chemistry

journal homepage: www.elsevier.com/locate/jelechem

Sensing electroadsorption reactions and surface mobility of electroadsorbed species by scanning electrochemical induced desorption

Mariela A. Brites Helú, Horacio L. Bonazza, José L. Fernández *

Programa de Electroquímica Aplicada e Ingeniería Electroquímica (PRELINE), Facultad de Ingeniería Química, Universidad Nacional del Litoral, Santiago del Estero 2829 (S3000AOM) Santa Fe, Santa Fe, Argentina

ARTICLE INFO

Article history:
Received 4 March 2016
Received in revised form 20 April 2016
Accepted 18 May 2016
Available online xxxx

Keywords:
SECM
Electro-adsorption
Surface diffusion
Hydrogen adsorption

ABSTRACT

A theoretical analysis of electro-adsorption reactions and of the surface diffusion of electro-adsorbed species based on scanning electrochemical microscopy (SECM) in the feedback mode, usually known as scanning electrochemical induced desorption (SECMID), is presented. Numerical simulations of the classical feedback process were carried out by including in the model a potential-dependent electro-adsorption reaction from the mediator at the substrate and allowing the adsorbed species (A_{ad}) to diffuse over the substrate surface affecting the mediator loop. As in classical SECMID, the local variation of the mediator concentration underneath the tip causes a potential-dependent gradient of the A_{ad} surface coverage at the substrate over the tip-affected region, which drives the A_{ad} surface diffusion toward this area and the consequent positive feedback of mediator, reaching a steady state. The simulated steady-state dependences of the tip current (i_T) on the substrate potential (E_S) show the presence of a peak over the potential range affected by the electro-adsorption reaction, whose amplitude at a given tip-substrate distance is mostly influenced by the surface diffusion coefficient of A_{ad} and the density of adsorption sites at the substrate. When this surface process is parallel to an electrode reaction of the mediator that proceeds over the same potential range, the adsorption/diffusion peak is overlapped with the typical Butler-Volmer type response of the electrode reaction, affecting the $i_T(E_S)$ shape and interfering with the determination of kinetic parameters from this dependence. These phenomena were experimentally observed when using the H^+/H_2 mediator loop on Au and Pt, where H_{ad} is electro-adsorbed from H^+, a process that in the case of Pt is parallel to the oxidation of the tip generated H_2.

1. Introduction

Scanning electrochemical microscopy (SECM) is nowadays a well-established powerful electrochemical technique thoroughly used to gain information on a great number of surface processes [1]. Among the many variants of the technique created to address different applications, one that emerged almost with the introduction of the technique is the so-called scanning electrochemical microscopy induced desorption (SECMID) [2]. This operation approach, which is based on the conventional feedback mode of SECM, allows measuring kinetics of adsorption/desorption reactions and rates of surface diffusion of adsorbed species [2]. SECMID and its variants were employed to study the behavior (i.e. the surface mobility) of species such as proton and others that were adsorbed on single-crystalline oxide surfaces [2] and on self-assembled monolayers [3–5]. As it was theoretically and experimentally demonstrated in these studies, the feedback of a mediator that involves an adsorbed participant is locally affected by the gradient of surface concentration of adsorbed species (or gradient of surface coverage) that develops on the substrate surface around the tip-affected area [2]. Thus, both the transient and the steady-state feedback approach curves contain information on the adsorption process and on the surface transport of the adsorbate. However, this operation mode was only barely considered in studies of electro-adsorption reactions and electro-adsorbed species [5]. The analysis of steady-state dependences of the feedback tip current on the substrate potential and on the tip-substrate distance could be potentially useful for measuring electro-adsorption parameters such as surface density of sorption sites, surface diffusion coefficient of an adsorbate, rate constant of an electro-adsorption reaction, among others. Moreover, the potential effects of adsorption processes on SECM voltammetric responses is lately receiving increasing attention due to the great deviation from the expected model behaviors that can be caused by this type of processes [6]. Thus, such analysis should also be important to understand the effect that an electro-adsorption reaction could have on the feedback loop of a redox mediator in solution that is used to investigate the kinetics of an electrode reaction at the substrate.

Electro-adsorption reactions are common reactions in electrocatalytic processes. An emblematic example is the electro-adsorption of atomic hydrogen (H_{ad}) from H^+ through reaction (1), which proceeds along with the hydrogen electrode reaction (HER).

* Corresponding author.
E-mail address: jlfernan@fiq.unl.edu.ar (J.L. Fernández).

http://dx.doi.org/10.1016/j.jelechem.2016.05.031
1572-6657/

$$H^+ + e^- \leftrightarrows H_{ad} \quad (1)$$

In fact, this is an important surface process with many implications in fundamental and technological electrochemical topics including not only electrocatalysis [7], but also corrosion [8], modified electrodes (for example with self-assembled monolayers [9]), among many others. Most conductive materials are capable to electro-adsorb atomic hydrogen through reaction (1), and the resulting H_{ad} could have different roles in a given electrocatalytic process depending on the particular situation. For example, the species H_{ad} may be simple spectators during the course of an electrochemical reaction, as are the under-potential deposited H (H_{UPD}) on Pt during the HER [7,10,11], which are electro-adsorbed over a potential range anodic respect to the equilibrium potential of the HER. These H_{UPD} may also participate as inhibitors of reaction sites of other reactions, as it happens during the 4 — e^- oxygen reduction on noble metals at cathodic potentials [12,13]. Moreover, the species H_{ad} may also participate as key intermediate species in the mechanism of an electrode reaction, as for example the over-potential deposited H (or H_{OPD}) in the HER [10,11], and as an important reactant in electrochemical hydrogenation of organic molecules [14]. Thus, the surface behavior of H_{ad} is likely to significantly affect the performance of many electrode reactions.

In the described context, this communication reports a theoretical study of the expected steady-state potential-dependent feedback responses of SECMID when an electro-adsorption reaction proceeds at the substrate affecting the mediator loop. The importance of this type of analysis is exemplified with SECM results measured on gold and platinum electrodes for the electro-adsorption of H_{ad} from H^+ through the reaction (1) and its surface diffusion.

2. Theory

The electrode reaction of a generic species O in solution that is electro-reduced at the substrate to an adsorbed species A_{ad} through reaction (2) was considered, where k_a^{app} and k_d^{app} are the potential dependent apparent electro-adsorption and electro-desorption rate constants [15].

$$O_{(dis)} + e^- \underset{k_d^{app}}{\overset{k_a^{app}}{\rightleftarrows}} A_{ad} \quad (2)$$

The two scenarios that are schematized in Fig. 1 were theoretically analyzed by mean of simulations.

The situation shown in Fig. 1a was proposed to explore the effect that the surface process by itself produces on the dependences of the tip current (i_T) vs. substrate potential (E_S) and tip-substrate distance (d), usually known as "working curves". A complete analysis of this case would permit to have a good overview on the potentiality of using $i_T(E_S, d)$ dependencies for measuring kinetic or equilibrium parameters of electro-adsorption reactions and of surface diffusion of the electro-adsorbed species. The second situation schematized in Fig. 1b was proposed to analyze the possible effects on the working curves of the surface processes occurring parallel to an electrode reaction with dissolved species. This should be useful to understand to what extent this phenomenon may interfere with the determination of kinetic parameters of the studied electrode reaction from fitting the feedback $i_T(E_S, d)$ dependences. The configuration shown in Fig. 1b is more general and includes the case of Fig. 1a as a particular condition where the rate of the electrode reaction at the substrate is null. Thus, the general model presented in Fig. 1b is developed below.

The theoretical model of Fig. 1a is essentially identical to that initially proposed by Unwin and Bard for the SECMID studies [2], but an E_S-dependent adsorption rate is involved in this case. Besides, in order to complete the model described in Fig. 1b, both the diffusion in solution of tip-generated species R and the electrode reaction at the substrate

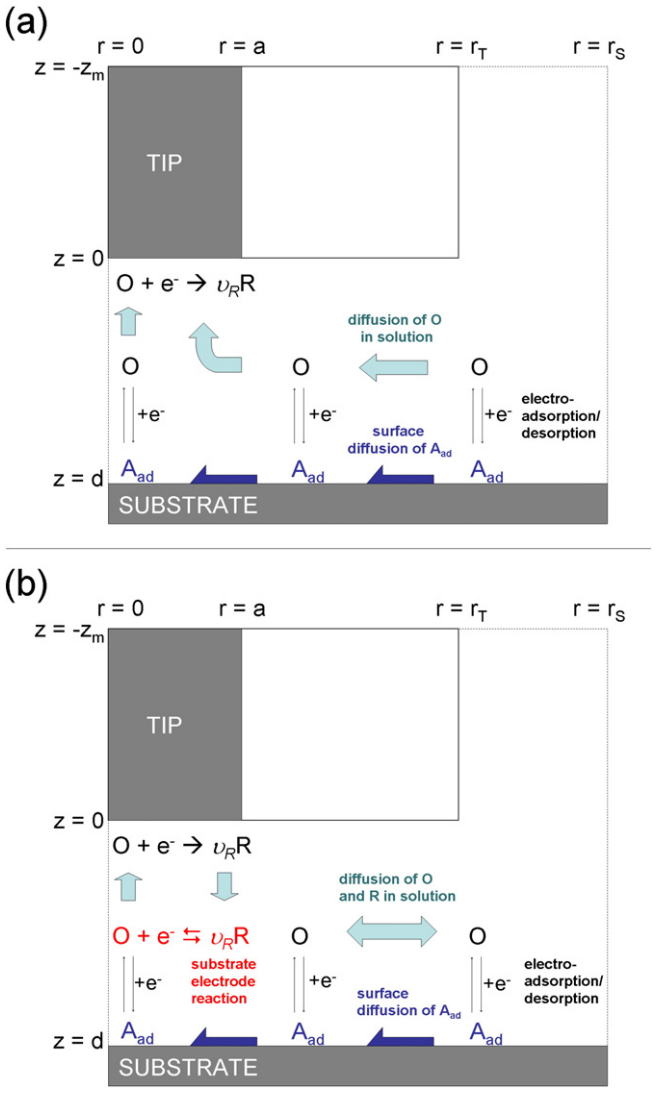

Fig. 1. Schematics of the two SECMID situations that were analyzed in this work.

indicated in Eq. (3) should be taken into account. Then, the dependences of the concentrations of species O (c_O) and R (c_R) with time (t) and position (r and z in cylindrical coordinates) are given by Eqs. (4) and (5), where D_i (in $cm^2\ s^{-1}$) is the diffusion coefficient of species i (O or R) in solution.

$$\upsilon_R R_{(dis)} \leftrightarrows O_{(dis)} + e^- \quad (3)$$

$$\frac{\partial c_O}{\partial t} = D_O\left(\frac{\partial^2 c_O}{\partial r^2} + \frac{\partial c_O}{r\partial r} + \frac{\partial^2 c_O}{\partial z^2}\right) \quad (4)$$

$$\frac{\partial c_R}{\partial t} = D_R\left(\frac{\partial^2 c_R}{\partial r^2} + \frac{\partial c_R}{r\partial r} + \frac{\partial^2 c_R}{\partial z^2}\right) \quad (5)$$

Furthermore, assuming Langmuir isotherm for modeling the electro-adsorption reaction (15), the initial and boundary conditions are defined by Eqs. (6) to (11).

$$t = 0: \quad 0 \le z \le d \text{ and } 0 \le r \le r_s,\ -z_m \le z \le 0 \text{ and } r_t \le r \le r_s: \quad c_O(r,z) = c_O^*;\ c_R(r,z) = 0 \quad (6)$$

$$z = d \text{ and } 0 \le r \le r_s: \quad \theta = \frac{c_O^* K_{ad}(E_S)}{1 + c_O^* K_{ad}(E_S)} \quad (7)$$

$$t>0: \quad z=0 \text{ and } 0\le r\le a: \quad c_O(r,z=0)=0; \quad c_R(r,z=0) = \left(\frac{D_O}{\upsilon_R D_R}\right)c_O^* \tag{8}$$

$$z=d \text{ and } 0\le r<r_s: \quad N\left(\frac{\partial\theta(r)}{\partial t}\right) = ND_A^s\left[\frac{\partial^2\theta(r)}{\partial r^2}+\left(\frac{1}{r}\right)\frac{\partial\theta(r)}{\partial r}\right]+\nu_{ad}(r) \tag{9}$$

$$D_O\frac{\partial c_O(r,z=d)}{\partial z}\Big)_{z=d} = \nu_{ad}(r)+\nu_{er}(r) \tag{10}$$

$$\upsilon_R D_R\frac{\partial c_R(r,z=d)}{\partial z}\Big)_{z=d} = -\nu_{er}(r) \tag{11}$$

In these equations, c_O^* is the bulk concentration of O (in mol cm^{-3}), θ is the fractional surface coverage of species A_{ad} that indicates the number of sites occupied by A_{ad} relative to the total number of sites on the surface, N is the surface density of adsorption sites (in mol cm^{-2}) that indicates the moles of total sites per unit area, D_A^s is the surface diffusion coefficient of A_{ad} (in cm^2 s^{-1}), ν_{ad} and ν_{er} (in mol cm^{-2} s^{-1}) are the rate of the electro-adsorption reaction and of the electrode reaction, respectively, at the radial coordinate r on the substrate surface. $K_{ad}(E_S)$ is the potential dependent equilibrium constant of the adsorption reaction, given by Eq. (12), where $f = F/RT$, k_a and k_d (in cm s^{-1}) are the forward (adsorption) and backward (desorption) rate constants of reaction (2).

$$K_{ad}(E_S) = \frac{k_a^{app}}{k_d^{app}} = \left(\frac{k_a}{k_d}\right)e^{-fE_S} \tag{12}$$

Other boundary conditions that apply at $r = 0$, at $r = r_s$, at $z = -z_m$, and on the insulating tip sheath surface are identical to the previously reported [2]. It can be seen from Eqs. (10) and (11) that at the substrate surface the diffusive flux of O is related to the adsorption and to the electrode reaction, while the diffusive flux of R is only related to the electrode reaction. Even though the rate of the electro-adsorption can be expressed in terms of $c_O(r, d)$, of $\theta(r)$ and of the potential-dependent rate constants as it was done in ref. [2], this work will consider only the particular case of a fast adsorption reaction that can be considered always at equilibrium (reversible). In this case, Eq. (13) relates $\theta(r)$ with $c_O(r, d)$ and with E_S, where E^* is an arbitrary reference potential and θ^* is the equilibrium coverage of A_{ad} at E^* that results from Eq. (7).

$$\theta(r) = \frac{\left(\frac{c_O(r,d)}{c_O^*}\right)}{\left(\frac{1-\theta^*}{\theta^*}\right)e^{f(E_S-E^*)}+\left(\frac{c_O(r,d)}{c_O^*}\right)} \tag{13}$$

Moreover, independently of the complexity of the electrode reaction mechanism, for simplicity the rate of the electrode reaction can be approximated by Eq. (14) [16] in terms of the kinetic parameters of a single-step reaction with a single standard rate constant (k^0 in cm s^{-1}), symmetry factor (α) and standard potential (E^0). As this equation is referred to E^0, a potential shift respect to the previously defined reference potential ($\Delta E = E^* - E^0$) is included for convenience. Thus, the value of ΔE indicates the extension of the potential overlapping between both reactions.

$$\nu_{er}(r) = k^0\left[c_O(r,d)e^{-\alpha f(E_S-E^*+\Delta E)} - c_R(r,d)e^{(1-\alpha)f(E_S-E^*+\Delta E)}\right] \tag{14}$$

The tip current (i_T) can be calculated from Eq. (15) as a function of E_S and d.

$$i_T = nFD_O\int_0^a 2\pi r\frac{\partial c_O(r,0)}{\partial z}\Big)_{z=0}dr \tag{15}$$

3. Experimental

3.1. Chemicals and materials

Lithium perchlorate (Merck, Germany) and perchloric acid (70%, Merck) were of analytical grade and used as received. Water used to prepare solutions was deionized with an exchange resin, doubly distilled, and treated with a Purelab purifier (Elga Labwater, resistivity ≥ 18.2 MΩ cm).

3.2. Instrumentation

Scanning electrochemical microscopy experiments were carried out using a home-built SECM instrument described elsewhere [17].

3.3. Electrodes

SECM disk-shaped tips (25 μm diameter) were fabricated by the conventional procedure of heat-sealing Pt or Au wires in borosilicate glass capillaries under vacuum, followed by polishing and sharpening [18]. A commercial mono-oriented Au(111) substrate grown on mica (Agilent Technologies, Santa Clara, CA) was flame-annealed under a hydrogen flame prior to be used. The polycrystalline Pt substrate was a Pt foil (Vega & Camji, Argentina) with 0.3 mm thickness. A Reversible Hydrogen Electrode (RHE) made in situ in the same solution was used as reference electrode. Pt or Au wires (1 mm diameter) were used as counter-electrodes.

3.4. SECM experiments

Steady-state $i_T(E_S)$ curves were measured at different tip-substrate distances on Pt and Au substrates using the H^+/H_2 mediator loop in deaerated 0.02 M $LiClO_4$–0.1 M $HClO_4$ under a nitrogen environment, employing Pt or Au tips and counter-electrodes, respectively. When studying the Pt substrate, a Pt tip was approached at a tip potential $E_T = -0.7$ V vs. RHE and $E_S = 0.6$ V vs. RHE, measuring the positive feedback current for the diffusion-limited proton reduction [19]. When studying the Au substrate, a Au tip was approached at a tip potential $E_T = -1.3$ V vs. RHE and $E_S = 0.8$ V vs. RHE, measuring a negative feedback approach curve for proton reduction. Both approach curves were properly fitted with the theoretical expressions for total positive or total negative feedback [1], respectively, which allowed to know the tip-substrate distances during the acquisition of $i_T(E_S)$ curves. Once the tip was positioned at a certain tip-substrate distance, the steady state $i_T(E_S)$ curve was measured by a slow potentiodynamic scan at −1 mV s^{-1} of the substrate potential from anodic (0.6 V vs. RHE for Pt and 0.9 V vs. RHE for Au) to cathodic (−0.25 V vs. RHE for Pt and −0.3 V vs. RHE for Au) values while keeping the tip potential at −0.7 V for Pt or −1.3 V for Au.

4. Results and discussion

4.1. Simulated $i_T(E_S, d)$ dependencies

In this work the simulated $i_T(E_S, d)$ dependencies in steady state where obtained by solving the time-dependent equations by an iterative explicit finite difference method [20,21]. Details of the application of this method to the general SECM model are given elsewhere [22], and the incorporation of the adsorption and surface diffusion boundary conditions to this algorithm is relatively straightforward. The steady-state dependences of the tip current normalized respect to the tip current at infinite distance ($I_T = i_T / i_{T,\infty}$, where $i_{T,\infty} = 4\beta_{RG}nFD_Oc_O^*a$ [1] is the tip current far away from the substrate and β_{RG} is the correction factor for the finite insulator thickness of the tip) on E_S were simulated using dimensionless variables ($R = r/a$, $Z = z/a$, $C_i = c_i/c_O^*$, $\tau = tD_O/a^2$) for varied normalized ($L = d/a$, $\gamma = N/c_O^*a$, $\xi_A = D_A^s/D_O$,

$\xi_R = \upsilon_R D_R / D_O, \kappa^0 = k^0 a / D_O$) and regular ($\theta^*, \Delta E$) parameters. In all simulations a value of $\theta^* = 0.5$ was set, so that E^* corresponds to this equilibrium coverage. Moreover, it was always assumed that $D_R = D_O$ and the stoichiometric coefficient $\upsilon_R = 0.5$, resulting $\xi_R = 0.5$. The steady-state condition at a certain pair of E_S and L values was set when no changes on time were detected for the calculated concentrations and coverage values ($\partial C_i / \partial \tau = 0$ and $\partial \theta / \partial \tau = 0$). The calculations started from an anodic E_S value that was kept during a quiet time ($\tau_{qt} = 100$) and the E_S value was changed every steps of -0.01 V with step times $\tau_{step} = 50$. It should be noted that in conditions where the rate constant of the electrode reaction is finite ($\kappa^0 > 0$), at $E_S < E^0$ the shielding effect should be important [22,23] and a true steady state cannot be reached.

The first situation that was explored is that schematized in Fig. 1a (null rate for the electrode reaction, or $\kappa^0 = 0$). The simulated $I_T(E_S, L)$ curves that resulted for a selected value of the product $\gamma\xi_A$ are shown in Fig. 2. The most important observation is the presence of a peak in the steady state $I_T(E_S)$ dependency, which develops over the negative feedback tip current. This steady-state positive feedback contribution is caused solely by the regeneration of O through reaction (2) at the substrate, which is sustained by the replenishment of the A_{ad} coverage by surface diffusion from the substrate region unaffected by the tip. As it is shown in Fig. 3a, a potential dependent radial gradient of θ develops on the substrate, which results from Eq. (13) due to the radial change of O concentration on the substrate surface caused by the tip reaction. This coverage gradient leads to a surface flux density of A_{ad} $J_A^s(R) = j_A^s(r) / D_O c_O^*$, where $j_A^s(r) = -N D_A^s \partial\theta(r) / \partial r]_r$, from the periphery to the center of the tip-affected substrate region (shown in Fig. 3b), and causes a steady-state flux of O from the substrate surface mostly focalized underneath the tip. The θ gradient is strongly sensitive to the substrate potential at potentials around the E^* value, where according to Eq. (13) θ is more sensitive to the O concentration. Thus, the surface flux is maximized at a substrate potential where A_{ad} coverage underneath the tip results much smaller than its outlying value, defining a maximum in the tip feedback current. Thus, the peak maximum is located at a substrate potential near the E^* value, although it slightly shifts toward more cathodic values as L decreases.

As it is shown in Fig. 4 the amplitude of the peak in the $I_T(E_S, L)$ curve strongly depends on the product $\gamma\xi_A$. Thus, the peak convolutes contributions of γ and ξ_A, and at a certain fixed L value an increase of γ should be evidenced by an increase of the peak current. However, a similar increase may also be caused by a higher mobility of A_{ad} (or a larger ξ_A value). Even though it is impossible to separate both contributions from steady state responses, it should be important to note that γ is a parameter that can be measured by an independent electrochemical technique, such as cyclic voltammetry, allowing the estimation of ξ_A (and D_A) from SECM working curves.

The second analyzed situation is that schematized in Fig. 1b with a finite rate constant ($\kappa^0 > 0$) for an electrode reaction with $\upsilon_R = 0.5$. The simulated $I_T(E_S)$ working curves that resulted using different values of the product $\gamma\xi_A$ for two different κ^0 values are shown in Fig. 5. The corresponding working curves simulated in absence of surface diffusion are included (open symbols) for a better appreciation of the effect that this surface process has on the SECM feedback response.

The first important aspect that can be observed in these simulations is that the surface diffusion peak appears lying on top of the working curve of the electrode reaction. However, such overlapping is not the result of a simple addition of both separated responses. In fact, it is verified that as the electrode reaction becomes faster, the term $\gamma\xi_A$ must become larger to clearly identify the surface diffusion peak that affects the working curve. This is reasonable since a faster electrode reaction tends to restore the concentration of O at the substrate surface more efficiently and over a potential range closer to the standard potential, causing the uniformization of the A_{ad} coverage and so decreasing the surface flux density. Thus, a larger mobility of A_{ad} and/or a larger surface density of adsorption sites are required to produce a surface flux density with detectable effects on the feedback of the O mediator.

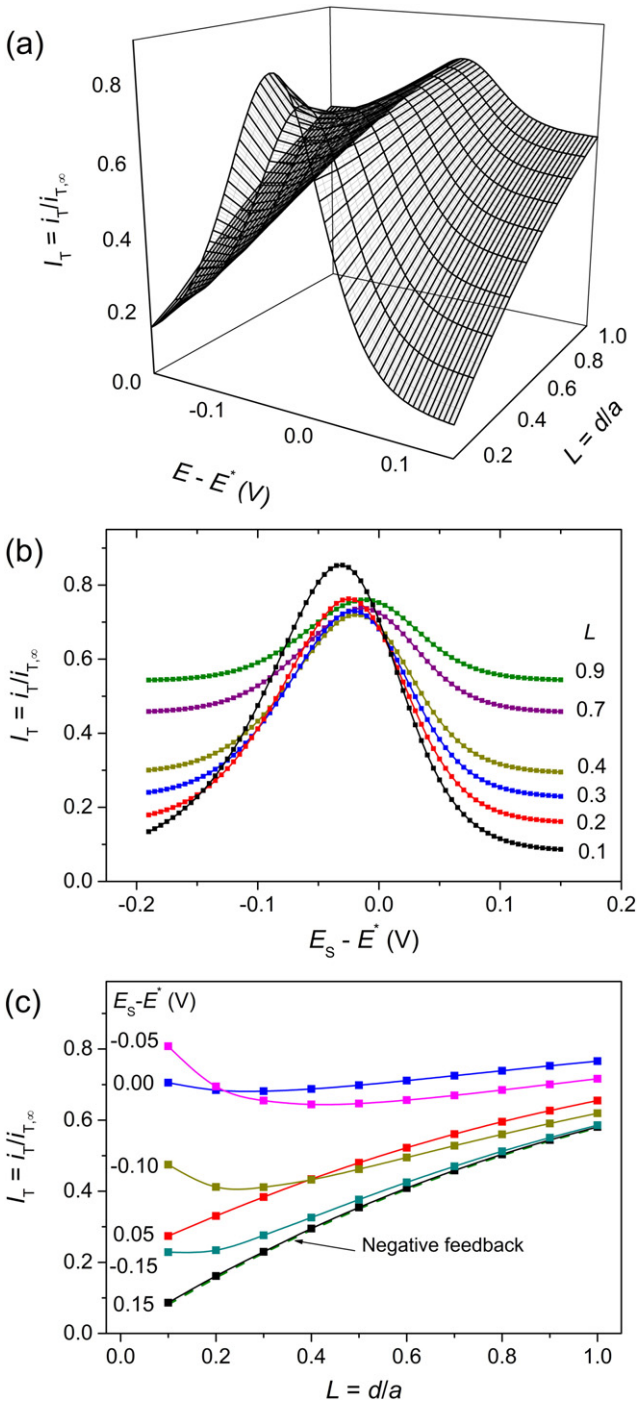

Fig. 2. (a) 3D representation of the SECM $I_T(E_S, L)$ dependence simulated with $\gamma\xi_A = 2$ and $\kappa^0 = 0$. (b) Projections of the $I_T(E_S)$ at different L values indicated within the graph. (c) Projections of the $I_T(L)$ at different E_S values indicated within the graph.

The peak maximum shows up at a potential slightly cathodic to the E^* value ($E^* = E^0 + 0.1$ V in Fig. 5), so that in this case the value of ΔE also affects the relative position of the peak and the peak amplitude as well, as it is observed in Fig. 6. At both extremes of ΔE (too negative or too positive) the surface diffusion peak is canceled. For too positive ΔE values (in this case for $\Delta E > 0.15$ V) the total positive feedback causes that $c_O(z = d, r) \cong c_O^*$. For too negative ΔE values (in this case for $\Delta E < -0.1$ V) the shielding process [22,23] causes that $c_O(z = d, r) \cong 0$ because the electrode reaction at the substrate is driven in the same direction than in the tip. In both cases the homogenization of $c_O(z = d, r)$ over the substrate surface causes a decrease of the θ gradient. Thus, the

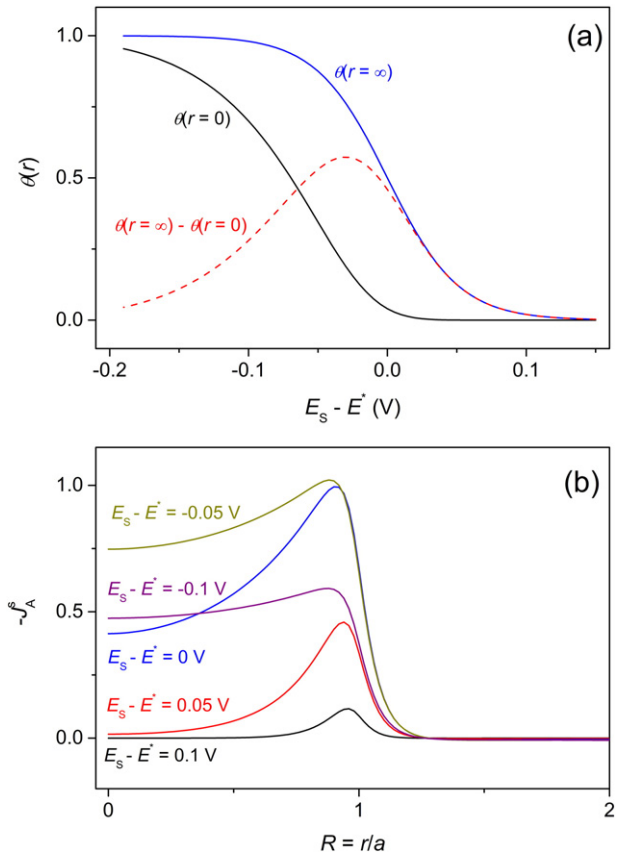

Fig. 3. (a) Coverage of A_{ad} at the substrate calculated as a function of the substrate potential right under the tip ($r = 0$) and far away from the tip affected region ($r = \infty$). The difference between these two curves is also shown (dashed line). (b) Normalized surface flux density of A_{ad} on the substrate surface as a function of the radius and of the substrate potential. In both figures the curves were simulated for $L = 0.1$, $\gamma\xi_A = 2$ and $\kappa^0 = 0$.

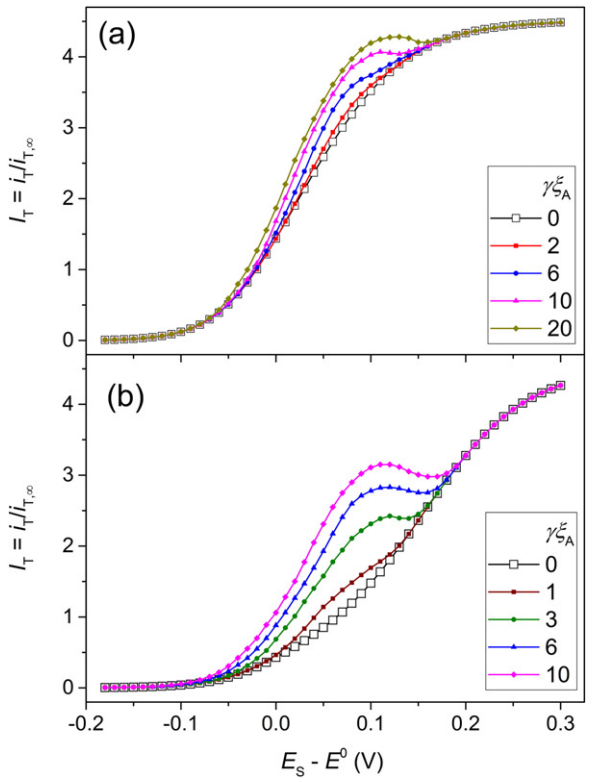

Fig. 5. Simulated $I_T(E_S)$ curves showing the effect of $\gamma\xi_A$ for values of $\kappa^0 = 1$ (a) and 0.1 (b). $\Delta E = E^* - E^0 = 0.1$ V. $L = 0.2$. The curves simulated in the absence of surface diffusion are included (open symbols).

surface diffusion peak is only clearly detected from the feedback curve for ΔE values between these two extreme situations. Then, in the cases of very fast electrode reactions with large rate constants that pass from total positive feedback to total shielding situations in a very short potential range, a parallel surface diffusion process would hardly affect the working curves.

The magnitude of the distortion caused on the $I_T(E_S)$ curve by the adsorption peak (respect to that expected for a single electrode reaction) strongly depends on the tip-substrate distance, as it is seen in Fig. 7. When the tip is too far away from the substrate ($L > 0.4$ for the conditions used in Fig. 7) the peak is practically undetectable from the working curve. As L decreases the adsorption peak grows and is clearly detected over the response of the electrode reaction, although the highest contrast between both processes is observed at intermediate distances, and not necessarily at the closest proximity (as the response of the electrode reaction becomes preponderant at smaller distances and the peak turns into just a shoulder).

These results show that an electro-adsorption process occurring in parallel to an electrode reaction studied by the feedback mode of SECM in steady state may interfere with the determination of the kinetic parameters as long as at least one of the species involved in the electro-adsorption reaction participates in the mediator loop. For fast electrode reactions this interference will be important when the adsorption process proceeds over the potential interval $E^0 \pm 0.1$ V and the surface mobility of the adsorbed species and/or the surface density of adsorption sites are high. If the electrode reaction is slow the potential interval where the adsorption process affects the measurement becomes

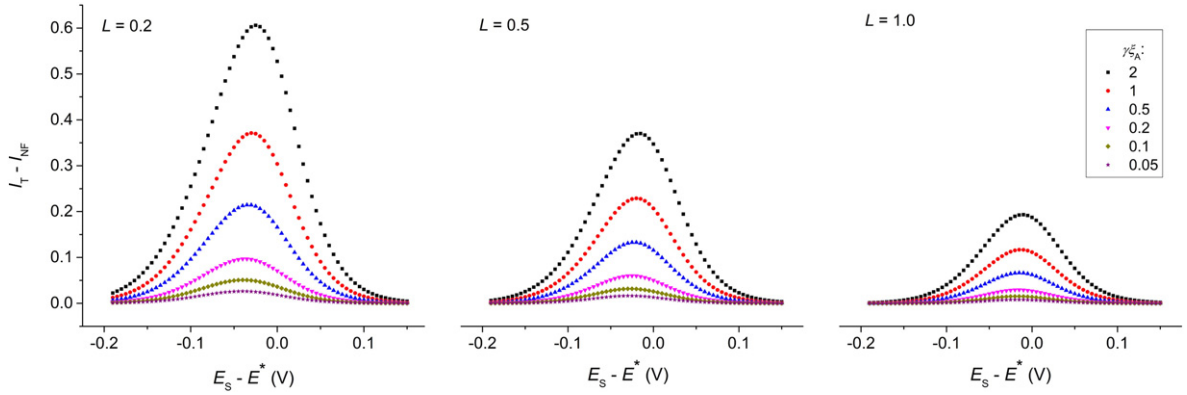

Fig. 4. Effect of $\gamma\xi_A$ on the simulated $I_T(E_S, L)$ dependence. The negative feedback current at each distance (I_{NF}) was subtracted from the I_T values. $\kappa^0 = 0$.

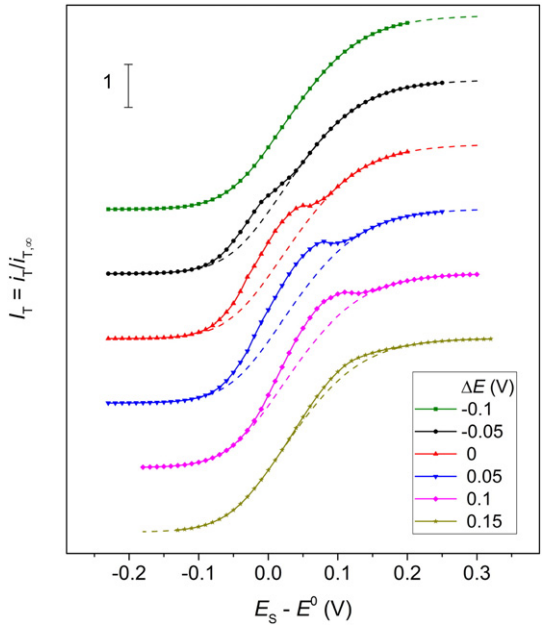

Fig. 6. Simulated $I_T(E_S)$ curves showing the effect of $\Delta E = E^* - E^0$ for $\gamma\xi_A = 10$, $\kappa^0 = 1$, and $L = 0.2$. Y-axes of each curve are shifted for a better appreciation of the effect. The curve simulated in the absence of surface diffusion is included (dashed line).

wider. While there could be a chance to use these curves as a mean for obtaining the adsorption and surface diffusion parameters through the correlation of experimental curves with simulations resulting from the complete model, this surely will not be straightforward. It is clear that these parameters along with those of the electrode reaction play complex roles in the definition of the resulting working curve, which makes difficult to find the right set of parameters that should lead to the simulated curves that better reproduce experimental results.

4.2. Surface diffusion of electroadsorbed H_{ad} on mono-oriented films of Au(111)

The H^+/H_2 couple is a suitable mediator to study the electroadsorption of H_{ad} on a substrate through reaction (1), which could occur parallel to the hydrogen oxidation reaction (*hor*) as long as the substrate is active enough for this reaction. In particular, the performance of gold for the *hor* still is not completely well understood, since the *hor* reaction rate and the sorption of H on this metal seems to be strongly affected by the pretreatment of the Au surface [24–27] and by the presence of Pt traces [28]. In the case of an untreated gold substrate, the rate of the *hor* in acid media is undetectable by SECM, but the adsorption of atomic hydrogen on gold (an issue deeply investigated at present [29–31]) is likely to occur only on certain types of sites [30,31]. On that sense, it has been suggested that H_{ad} is only adsorbed on deficiently coordinated Au atoms located at plane borders and edges [30,31] and is not adsorbed on Au atoms of terraces. Thus, any positive feedback caused by regeneration of H^+ at the substrate should come only from reaction (1) fed by the surface diffusion of any H_{ad} generated at the Au surface (case shown in Fig. 1a).

In this context, the adsorption and surface diffusion of H on mono-oriented Au(111) films deposited on mica was analyzed. As compared with the polycrystalline metal, this reconstructed surface presents a large fraction of Au atoms at the (111) terraces and a very small percentage of reactive Au sites at the step edges and defects. Typical $I_T(E_S)$ curves measured in steady state by slow potentiodynamic scans at different L values are shown in Fig. 8. At E_S values larger than 0.7 V vs. RHE the current corresponds to the pure negative feedback current for each distance, indicating undetectable activity of Au for the *hor* over the analyzed potential range. For the closest distances, a steady state peak can be clearly detected over this negative feedback current in the range $0\ V < E_S$ vs. RHE < 0.6 V, which is likely caused by the surface diffusion of electroadsorbed H_{ad}. Besides, at E_S values more negative than -0.1 V vs. RHE the current decreases to near zero due to hydrogen evolution at the substrate causing the depletion of the proton concentration [19,23].

The $I_T(E_S)$ curve measured at the closest distance ($L = 0.28$) (curve d) presents a peak with a maximum amplitude $I_{peak,max} = I_{T,max} - I_{NF} \cong 0.05$, which according to the simulations would match a situation with $\gamma\xi_A < 0.1$, which indicates a very small density of adsorption sites and/or low mobility of H_{ad}. It is important to note that peaks for electroadsorption of H are only barely detected by cyclic voltammetry on polycrystalline Au, even when using expanded current scales [27], so that γ should be very small. Moreover, the experimental peak width of about 0.3 V at the base is larger than that observed in the simulated curves (<0.2 V). This could be indicative of the presence of multiple peaks with slightly different E^* values convoluted in an apparently single peak. It is also possible that the kinetics of the adsorption reaction is not very fast or the adsorption reaction deviates from the Langmuir-type behavior, and this affects the peak shape. On the other hand, the peak potential value is around 0.35 V vs. RHE, which is quite anodic for H electro-adsorption. Voltammetric peaks for H adsorption/desorption were detected close to these anodic potentials on single gold nanoparticles [32]. Besides, the reported voltammetric responses of adsorbed hydrogen on polycrystalline gold [25–27,33] indicate the strong

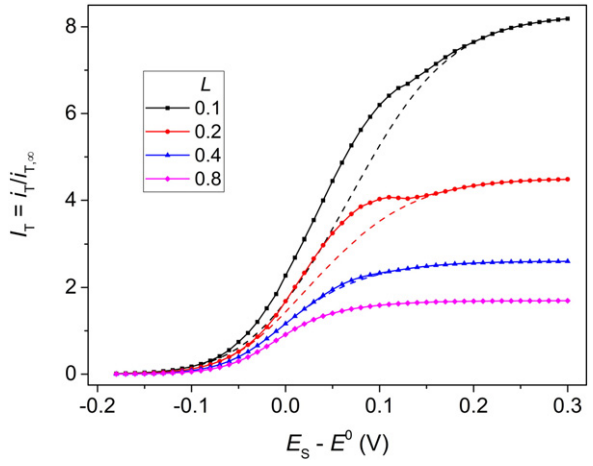

Fig. 7. $I_T(E_S)$ curves simulated at different tip-substrate distances for $\gamma\xi_A = 10$, $\kappa^0 = 1$, $\Delta E = 0.1$. Dashed lines are the curves simulated in the absence of surface diffusion.

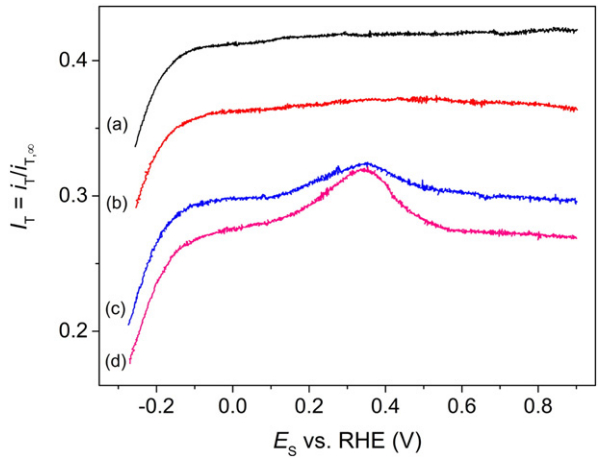

Fig. 8. Experimental $I_T(E_S)$ curves measured using the H^+/H_2 mediator in steady state at $L = 0.48$ (a), 0.4 (b), 0.32 (c), and 0.28 (d) on a Au(111)/mica substrate in 0.02 M $HClO_4$–0.1 M $LiClO_4$. Substrate potential scan rate: 1 mV s^{-1}.

sensitivity of this process to the surface state, and in particular to the presence of absorbed hydrogen [33] and adsorbed oxygen-based species (or incipient oxides) [25,26]. Thus, it is reasonable to think that reaction (1) on gold could be driven or mediated by these species.

The peak is not detected at L values larger than typically 0.4, although below this value the peak is clearly observed and its intensity increases notably as L decreases. Such dependence of the peak current on L is different to those obtained in the simulations for any value of $\gamma\xi_A$. If, as it was proposed [30,31], the H adsorption and surface diffusion processes are only operative onto the Au sites located at the crystalline edges, then the positive feedback only comes from these localized regions. Therefore, the feedback performance of this type of substrate should be better represented as an ensemble of interconnected active lines that would behave like nanobands with atomic widths. This type of substrate should have an $I_T(L)$ feedback dependence quite different to that of a continuous substrate, and should be strongly affected by the ratio between the bandwidth and the tip radius [34], particularly if this ratio is very small. Thus, the anomalous dependence of the peak current on L could be an indirect indication of adsorption and surface diffusion of H on Au steps and edges.

4.3. Surface diffusion of electroadsorbed H_{ad} on polycrystalline Pt

The *hor* on polycrystalline platinum substrate is a fast reaction that, when is studied by SECM, approaches to the total positive feedback condition at low overpotentials [19,35,36] (typically at $E_S > 0.2$ V vs. RHE). In this case, the electro-adsorption of H_{ad}, usually known as H_{UPD}, proceeds over the same potential range (0 V < E_S vs. RHE < 0.4 V) [19]. Thus, the positive feedback caused by regeneration of H^+ at the substrate comes both from the *hor* and from reaction (1) occurring simultaneously on different adsorption sites at the Pt surface (case shown in Fig. 1b with $\upsilon_R = 0.5$). In line with this, the transient dependence of I_T on E_S during a scan of the substrate potential was already used to probe reaction (1) [19,37] and to sense pH changes at the substrate surface due to electro-adsorption reactions [38]. In addition, based on the previously shown simulations, the steady state $I_T(E_S)$ dependences should also be sensitive to the *hor*, to reaction (1), and to the surface diffusion of H_{ad}. In this context, Fig. 9 shows $I_T(E_S)$ dependences measured using the H^+/H_2 mediator in steady state on a polycrystalline platinum substrate as described in the Experimental section using a platinum tip ($E_T = -0.7$ V vs. RHE) positioned at different tip-substrate distances.

The positive feedback of H^+ is detected at $E_S > 0$ V, and shielding of the substrate is verified below this E_S value as the incipient hydrogen evolution at the substrate produces a decay of the H^+ surface concentration [23]. The positive feedback tip current has contributions from the *hor* and from the electro-adsorption/surface diffusion of H_{ad}, which, according to the cyclic voltammogram of the Pt substrate in this media [37], actually involves at least two adsorption reactions occurring with different E^* values over the potential range 0 V < E_S vs. RHE < 0.4 V. Thus, the steady-state response for the *hor* over this potential interval is accompanied by at least two steady-state overlapped peaks, which are caused by the surface diffusion of the different types of H_{ad}. At the largest tip-substrate distances the peaks are practically undetected, although as the distance becomes smaller a single broad peak is clearly detected over the potential interval 0.05 V < E_S vs. RHE < 0.2 V. It should be pointed out that an equivalent result was reported previously [35] showing a maximum in the dependence of the SECM-determined *hor* rate constant on the substrate potential over this same potential interval. A second dim peak is barely detected at the closest distances in the potential range 0.25 V < E_S vs. RHE < 0.4 V, before the tip current reaches the limiting value at $E_S > 0.5$ V. It is clear that the adsorption of H affects the SECM steady-state response for the *hor*, so that the analysis of this reaction, and of any electrode reaction that proceeds in parallel with adsorption processes that can affect the mediator loop, should take into account this effect. While it is possible to make a qualitative interpretation of these curves based on the previously described model, a more quantitative correlation is not feasible due to the marked differences between the assumptions of the model and the real system. Thus for example, while the model involves only one adsorbed species with a characteristic E^* value, the real system includes several types of H_{ad} that adsorb at different potentials [39]. However, the lower intensity of the more anodic peak can be explained based on the results presented in Fig. 6, which show that as the E^* value approaches to the total positive feedback condition the peak intensity decreases. On the other hand, the model in this work is based on a single-step Butler-Volmer type reaction, while it is known that the *hor* operates through a three-step mechanism [11] that, in conditions of high mass transport rates such as those defined by SECM, can lead to particular SECM dependences that are impossible to be described by a single reaction, such as the attainment of a kinetic limiting current and the transition between mechanistic routes [40].

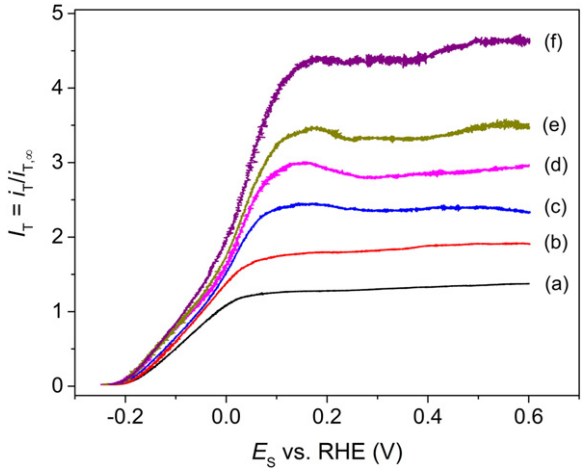

Fig. 9. Experimental $I_T(E_S)$ curves measured on a polycrystalline Pt substrate using the H^+/H_2 mediator at $L = 1.31$ (a), 0.64 (b), 0.45 (c), 0.34 (d), 0.27 (e), and 0.19 (f) in 0.02 M $HClO_4$–0.1 M $LiClO_4$.

5. Conclusions

In a typical feedback-based SECM experiment, the steady-state $i_T(E_S, d)$ dependence can be strongly affected by electro-adsorption reactions that involve the mediator as a reactant, in a similar way to other adsorption effects recently reported for varied SECM configurations [6]. While electro-adsorption is a transient process, a steady-state positive feedback current can be sustained by the surface diffusion of the electro-adsorbed species, which is driven by a radial gradient of surface coverage.

On the one hand, when only the electro-adsorption reaction is operative at the substrate, the adsorption/surface diffusion processes lead to a steady-state positive feedback current with a peak-shaped dependence on E_S, which is mounted on the negative feedback tip current. Thus, the steady-state $i_T(E_S, d)$ dependences are potentially useful for qualitative and quantitative characterization of surface processes, allowing for example the estimation of surface diffusion parameters. When this analysis was applied to investigate the electro-adsorption of H from H^+ on mono-oriented Au(111), solid evidences were taken that this reaction occurs only on a small fraction of sites, probably the plane edges, although a quantitative characterization was not possible with the developed model. Both the adsorption reaction and the SECM response may be affected by other proton-sensitive surface processes (i.e. reduction of gold oxide), which complicate the model and the quantification.

On the other hand, when the electro-adsorption reaction is simultaneous to an electrode reaction of the mediator that proceeds under mixed control over the same potential range, the adsorption/diffusion peak is overlapped with the typical SECM response of the electrode

reaction, affecting the $i_T(E_S)$ shape and disturbing the determination of kinetic parameters from $i_T(E_S, d)$ dependences using the classical SECM theoretical tools. The SECM analysis of the hydrogen oxidation on polycrystalline Pt presented in this work shows an example of this effect, which in this case is caused by the electroadsorption of under-potential deposited H over the same potential range where hydrogen oxidation is studied.

Acknowledgements

This work was supported by Agencia Nacional de Promoción Científica y Tecnológica (PICT 2014 2001), Consejo Nacional de Investigaciones Científicas y Técnicas (PIP 112-201101-00674) and Universidad Nacional del Litoral (CAI+D 501-201101-00333 LI).

References

[1] A.J. Bard, M.V. Mirkin (Eds.), Scanning Electrochemical Microscopy, second ed.CRC Press, Boca Raton, 2012.
[2] P.R. Unwin, A.J. Bard, Scanning electrochemical microscopy. 14. Scanning electrochemical microscope induced desorption: a new technique for the measurement of adsorption/desorption kinetics and surface diffusion rates at the solid/liquid interface, J. Phys. Chem. 96 (1992) 5035–5045.
[3] C.J. Slevin, P.R. Unwin, Lateral proton diffusion rates along stearic acid monolayers, J. Am. Chem. Soc. 122 (2000) 2597–2602.
[4] J. Zhang, C.J. Slevin, C. Morton, P. Scott, D.J. Walton, P.R. Unwin, New approach for measuring lateral diffusion in Langmuir monolayers by scanning electrochemical microscopy (SECM): theory and application, J. Phys. Chem. B 105 (2001) 11120–11130.
[5] L.H. Lie, M.V. Mirkin, S. Hakkarainen, A. Houlton, B.R. Horrocks, Electrochemical detection of lateral charge transport in metal complex-DNA monolayers synthesized on Si(111) electrodes, J. Electroanal. Chem. 603 (2007) 67–80.
[6] S. Tan, J. Zhang, A.M. Bond, J.V. Macpherson, P.R. Unwin, Impact of adsorption on scanning electrochemical microscopy voltammetry and implications for nanogap measurements, Anal. Chem. 88 (2016) 3272–3280.
[7] G. Jerkiewicz, Electrochemical hydrogen adsorption and absorption. Part 1: under-potential deposition of hydrogen, Electrocatalysis 1 (2010) 179–199.
[8] S. Lynch, Mechanistic and fractographic aspects of stress corrosion cracking, Corros. Rev. 30 (2012) 63–104.
[9] J. Kucera, A. Groß, Reduced Pd density of states in Pd/SAM/Au junctions: the role of adsorbed hydrogen atoms, Phys. Chem. Chem. Phys. 14 (2012) 2353–2361.
[10] B.E. Conway, G. Jerkiewicz, Nature of electrosorbed H and its relation to metal dependence of catalysis in cathodic H_2 evolution, Solid State Ionics 150 (2002) 93–103.
[11] M.R. Gennero de Chialvo, A.C. Chialvo, Recent progress in the kinetic analysis of the hydrogen electrode reaction in steady state, Curr. Top. Electrochem. 11 (2006) 1–11.
[12] N.M. Markovic, R.R. Adzic, B.D. Cahan, E.B. Yeager, Structural effects in electrocatalysis: oxygen reduction on platinum low index single-crystal surfaces in perchloric acid solutions, J. Electroanal. Chem. 377 (1994) 249–259.
[13] M.F. Li, L.W. Liao, D.F. Yuan, D. Mei, Y.-X. Chen, pH effect on oxygen reduction reaction at Pt(1 1 1) electrode, Electrochim. Acta 110 (2013) 780–789.
[14] R.P.S. Chaplin, A.A. Wragg, Effects of process conditions and electrode material on reaction pathways for carbon dioxide electroreduction with particular reference to formate formation, J. Appl. Electrochem. 33 (2003) 1107–1123.
[15] E. Gileadi (Ed.), Electrode Kinetics for Chemists, Chemical Engineers, and Materials Scientists, VCH, New York 1993, p. 266 (Chapter I).
[16] A.J. Bard, L.R. Faulkner, Electrochemical Methods – Fundamentals and Applications, second ed. Wiley, New York, 2001 109 (Chapter 3).
[17] H.L. Bonazza, L.D. Vega, J.L. Fernández, Analysis of the hydrogen electrode reaction mechanism in thin-layer cells. 2. Study of hydrogen evolution on microelectrodes by scanning electrochemical microscopy, J. Electroanal. Chem. 713 (2014) 9–16.
[18] F.-R.F. Fan, J.L. Fernández, B. Liu, J. Mauzeroll, C.G. Zoski, in: C.G. Zoski (Ed.), Handbook of Electrochemistry, Elsevier, Amsterdam 2007, pp. 189–197 (Chapter 6.3.1).
[19] J. Zhou, Y. Zu, A.J. Bard, Scanning electrochemical microscopy. Part 39. The proton/hydrogen mediator system and its application to the study of the electrocatalysis of hydrogen oxidation, J. Electroanal. Chem. 491 (2000) 22–29.
[20] J.L. Fernández, A.J. Bard, Scanning electrochemical microscopy. 50. Kinetic study of electrode reactions by the Tip Generation–Substrate Collection mode, Anal. Chem. 76 (2004) 2281–2289.
[21] J.L. Fernández, C. Hurth, A.J. Bard, Scanning electrochemical microscopy. 54. Application to the study of heterogeneous catalytic reactions – hydrogen peroxide decomposition, J. Phys. Chem. B 109 (2005) 9532–9539.
[22] C.G. Zoski, C.R. Luman, J.L. Fernández, A.J. Bard, Scanning electrochemical microscopy. 57. SECM tip voltammetry at different substrate potentials under quasi-steady-state and steady-state conditions, Anal. Chem. 79 (2007) 4957–4966.
[23] C.G. Zoski, J.C. Aguilar, A.J. Bard, Scanning electrochemical microscopy. 46. Shielding effects on reversible and quasireversible reactions, Anal. Chem. 75 (2003) 2959–2966.
[24] G.M. Schmid, Hydrogen overvoltage on gold, Electrochim. Acta 12 (1967) 449–459.
[25] R. Córdova Orellana, M.E. Martins, A.J. Arvía, Potentiodynamic oxidation of absorbed and adsorbed hydrogen atoms on gold promoted by the dynamic ageing of the oxygen containing layer, Electrochim. Acta 24 (1979) 469–471.
[26] M.E. Martins, J.J. Podestá, A.J. Arvía, Chemical evidence of hydrogen sorption processes on potential cycled gold electrodes, Electrochim. Acta 32 (1987) 1013–1017.
[27] M.G. Sustersic, N.V. Almeida, A.E. Von Mengershausen, Hydrogen oxidation on gold electrode in perchloric acid solution, Int. J. Hydrog. Energy 35 (2010) 6063–6068.
[28] J. Solla-Gullón, A. Aldaz, J. Clavilier, Ultra-low platinum coverage at gold electrodes and its effect on the hydrogen reaction in acidic solution, Electrochim. Acta 87 (2013) 669–675.
[29] K. Sun, M. Kohyama, S. Tanaka, S. Takeda, A study on the mechanism of H_2 dissociation on Au/TiO_2 catalysts, J. Phys. Chem. C 118 (2014) 1611–1617.
[30] D.A. Panayotov, S.P. Burrows, J.T. Yates Jr., J.R. Morris, Mechanistic studies of hydrogen dissociation and spillover on Au/TiO_2: IR spectroscopy of coadsorbed CO and H-donated electrons, J. Phys. Chem. C 115 (2011) 22400–22408.
[31] E. Bus, J.T. Miller, J.A. van Bokhoven, Hydrogen chemisorption on Al_2O_3-supported gold catalysts, J. Phys. Chem. B 109 (2005) 14581–14587.
[32] Y. Yu, Y. Gao, K. Hu, P.Y. Blanchard, J.M. Noël, T. Nareshkumar, K.L. Phani, G. Friedman, Y. Gogotsi, M.V. Mirkin, Electrochemistry and electrocatalysis at single gold nanoparticles attached to carbon nanoelectrodes, ChemElectroChem 2 (2015) 58–63.
[33] M.G. Sustersic, N.V. Almeida, A.E. Von Mengershausen, S.M. Esquenoni, Hydrogen oxidation on gold electrode in sulphuric acid solution, Int. J. Hydrog. Energy 37 (2012) 14747–14752.
[34] H. Xiong, D.A. Gross, J. Guo, S. Amemiya, Local feedback mode of scanning electrochemical microscopy for electrochemical characterization of one-dimensional nanostructure: theory and experiment with nanoband electrode as model substrate, Anal. Chem. 78 (2006) 1946–1957.
[35] K. Jambunathan, B.C. Shah, J.L. Hudson, A.C. Hillier, Scanning electrochemical microscopy of hydrogen electro-oxidation. Rate constant measurements and carbon monoxide poisoning on platinum, J. Electroanal. Chem. 500 (2001) 279–289.
[36] C.G. Zoski, Scanning electrochemical microscopy: investigation of hydrogen oxidation at polycrystalline noble metal electrodes, J. Phys. Chem. B 107 (2003) 6401–6405.
[37] Y.F. Yang, G. Denuault, Scanning electrochemical microscopy (SECM): study of the adsorption and desorption of hydrogen on platinum electrodes in Na_2SO_4 solution (pH = 7), J. Electroanal. Chem. 418 (1996) 99–107.
[38] Y.F. Yang, G. Denuault, Scanning electrochemical microscopy (SECM) study of pH changes at Pt electrode surfaces in Na_2SO_4 solution (pH 4) under potential cycling conditions, J. Chem. Soc. Faraday Trans. 92 (1996) 3791–3798.
[39] B.E. Conway, B.V. Tilak, Interfacial processes involving electrocatalytic evolution and oxidation of H_2, and the role of chemisorbed H, Electrochim. Acta 47 (2002) 3571–3594.
[40] J.L. Fernández, Analysis of the hydrogen electrode reaction mechanism in thin-layer cells. 1. Theory, J. Electroanal. Chem. 650 (2010) 90–97.